Nuclear Physics B343 (1990) 285–309
North-Holland

INVESTIGATION OF EXCLUSIVE CHANNELS IN $\nu/\bar{\nu}$-DEUTERON CHARGED CURRENT INTERACTIONS

Amsterdam–Bergen–Bologna–Padova–Pisa–Saclay–Torino Collaboration

D. ALLASIA[7], C. ANGELINI[5], G.W. van APELDOORN[1], A. BALDINI[5], S.M. BARLAG[1]*, L. BERTANZA[5], F. BOBISUT[4], P. CAPILUPPI[3], P.H.A. van DAM[1], M.L. FACCINI-TURLUER[6], A.G. FRODESEN[2], G. GIACOMELLI[3], H. HUZITA[4], B. JONGEJANS[1], G. MANDRIOLI[3], A. MARZARI-CHIESA[7], R. PAZZI[5], L. RAMELLO[7], A. ROMERO[7], A.M. ROSSI[3], A. SCONZA[4], P. SERRA-LUGARESI[3], A.G. TENNER[1], D. VIGNAUD[6]

[1]*NIKHEF-H, Amsterdam, The Netherlands*
[2]*Institute of Physics, University of Bergen, Norway*
[3]*Dipartimento di Fisica dell'Università di Bologna, INFN sezione di Bologna, Italy*
[4]*Dipartimento di Fisica dell'Università di Padova, INFN sezione di Padova, Italy*
[5]*Dipartimento di Fisica dell'Università di Pisa, INFN sezione di Pisa, Italy*
[6]*Département de Physique des Particules Elémentaires, CEN-Saclay, France*
[7]*Dipartimento di Fisica Sperimentale dell'Università, INFN sezione di Torino, Italy*

Received 15 January 1990
(Revised 27 April 1990)

An analysis has been performed of neutrino and antineutrino interactions with protons and neutrons in a deuterium bubble chamber. The interactions under study are quasielastic neutrino–neutron scattering and one-, two- and three-pion production reactions. Results are presented on cross sections, effective mass distributions, resonance production, momentum transfer distributions and coefficients of the decay angular distributions. Where possible, comparisons are made with existing theoretical models and predictions.

1. Introduction

In the present paper a study will be made of several exclusive channels in $\nu/\bar{\nu}$ interactions with protons and neutrons. The data were obtained from the WA25 experiment with the CERN bubble chamber BEBC filled with deuterium, exposed

* Now at KNMI, De Bilt, The Netherlands.

0550-3213/90/$03.50

to high-energy $\nu/\bar{\nu}$ beams at the CERN-SPS. The following interactions are studied:

(a) Quasielastic neutrino–neutron scattering:

$$\nu + \mathrm{n} \rightarrow \mu^- + \mathrm{p}. \tag{1}$$

(b) One-pion production in the baryon resonance region ($W < 2$ GeV/c^2, where W is the rest mass of the secondary hadronic system):

$$\nu + \mathrm{p} \rightarrow \mu^- + \mathrm{p} + \pi^+, \tag{2}$$

$$\bar{\nu} + \mathrm{n} \rightarrow \mu^+ + \mathrm{n} + \pi^-, \tag{3}$$

$$\bar{\nu} + \mathrm{p} \rightarrow \mu^+ + \mathrm{p} + \pi^-, \tag{4}$$

$$\nu + \mathrm{n} \rightarrow \mu^- + \begin{pmatrix} \mathrm{p} + \pi^0 \\ \mathrm{n} + \pi^+ \end{pmatrix}. \tag{5}$$

(c) Production of pions at low momentum transfer to the nucleon with $W >$ 2 GeV/c^2:

$$\nu + \mathrm{p} \rightarrow \mu^- + \mathrm{p} + \pi^+, \tag{6}$$

$$\bar{\nu} + \mathrm{p} \rightarrow \mu^+ + \mathrm{p} + \pi^-, \tag{7}$$

$$\nu + \mathrm{n} \rightarrow \mu^- + \mathrm{p} + \pi^+ + \pi^-, \tag{8}$$

$$\nu + \mathrm{p} \rightarrow \mu^- + \mathrm{p} + \pi^+ + \pi^+ + \pi^-, \tag{9}$$

$$\bar{\nu} + \mathrm{p} \rightarrow \mu^+ + \mathrm{p} + \pi^+ + \pi^- + \pi^-. \tag{10}$$

The cut in W at 2 GeV/c^2 divides the reactions (which partly have the same topologies) into classes in which different production mechanisms are prevailing.

Several experiments have studied one or more of the above given reactions at various incident energies. We quote refs. [1–5] for the quasi-elastic reaction, [2] and [6–13] for single-pion reactions and [11, 14] for multi-pion reactions. In this paper we give the characteristics of these reactions in a simultaneous analysis. Some of the analyzed reactions have not been investigated before. Part of the data has been presented in previous publications [15, 16]. The present paper covers the full statistics of the experiment.

Sects. 2–6 of this paper contain the description of the experimental methods and the physical variables to be obtained. In sect. 7 the cross-section measurement is described and the cross sections of the various channels are presented. In sect. 8 an analysis is made of the quasielastic ν–n scattering. Sect. 9 treats the production

of the baryon resonances decaying into a nucleon and a pion. Effective mass diagrams and differential distributions of cross sections are presented in this section, together with results on the decay angular distribution. In sect. 10 one-, two- and three-pion final states are analyzed outside the effective mass region of the baryon resonances.

2. The experiment

The data were obtained from various exposures of BEBC to neutrino and antineutrino wide-band beams. In total, 75,000 pictures were taken with neutrino and 272,000 with antineutrino beam setting. Protons of 400 GeV were incident on a Be target of 60 cm (ν) or 110 cm ($\bar{\nu}$) length. The beam was focussed by a horn and reflector system. The mean event energy amounted to 54 GeV for ν and 40 GeV for $\bar{\nu}$. A discussion of the event energy spectra is given in ref. [17]. The fiducial volume of the chamber amounted to 18.14 m^3, containing 2.52 tons of deuterium. The bubble chamber was equipped with an External Muon Identifier EMI and during part of the exposures with an Internal Picket Fence IPF. Charged current events were selected by means of the EMI by the identification of a negative or positive muon in the final state. The film was scanned twice for all topologies. In total, 27575 ν and 16896 $\bar{\nu}$ events were obtained with the two beam settings. For most of the present analysis all events were used. However, the cross-section determination was restricted to $\nu/\bar{\nu}$ events obtained with the specific $\nu/\bar{\nu}$ beam setting, as will be explained in sect. 7.

A special scan was performed to evaluate the scanning loss of the 2- and 3-prong topologies relevant to this paper.

3. Kinematics

All events with topological multiplicity below 6 were passed through the kinematics fit program. For reactions (1), (2), (4) and (6)–(10) a 3-constraint kinematical fit was required for the identification. The (anti)neutrino entered the fit procedure with an unmeasured momentum. The direction was chosen to be the nominal beam direction with 1 mrad errors in the polar and azimuthal angles. Special care had to be taken for the visible or invisible companion of the interacting nucleon in deuterium. In all cases the deuteron was considered the target particle. Visible spectator protons with a momentum larger than 150 MeV/c were measured as outgoing particles. Visible protons with smaller momentum were considered invisible since their measurement is not reliable. Invisible spectators were entered into the fitting procedure as a proton or a neutron with nominally zero momentum and momentum errors Δp in the x, y and z direction. Δp was set to 60 MeV/c for the neutron spectator in odd-prong events, where the target is a proton and to 30 MeV/c for the invisible proton spectator in even-prong

events. The smaller value of Δp was assigned in the second case, because spectators with a large momentum are visible and measurable. Kinematical fits with a probability below 1% were not accepted.

As a general check and to recover some failures in the standard method, a second method of kinematical analysis was applied in parallel. Events of the indicated topologies were selected as fitting candidates, when the total momentum of the secondaries transverse to the nominal beam direction was below 0.30 GeV/c and the missing energy was between -0.20 and $+0.14$ GeV. The limits allow for the Fermi motion of invisible spectators and the uncertainty in the neutrino direction. The separate study of momentum loss and energy loss among others facilitates the recovery of events that fail in the standard fit procedure because of a large momentum of a neutron spectator. By means of the second method the event samples are increased by $\approx 5\%$. Fig. 1 shows the missing energy distribution for the candidates of reaction (1) that satisfy the transverse momentum criterion. The applied energy cuts are indicated in the figure.

In cases, where a fit with non-strange charged particles was ambiguous with one containing strange particles, the first one was preferred. All neutral particles, including gammas, that seemed to be connected with the primary interaction, were fitted to the vertex. In the case of a successful fit the event was rejected, with the exception of candidates for reaction (5a) where one or two fitting γ's were accepted. No fits were accepted with mass assignments different from the ones made on the basis of bubble density at the scanning table. At low momentum

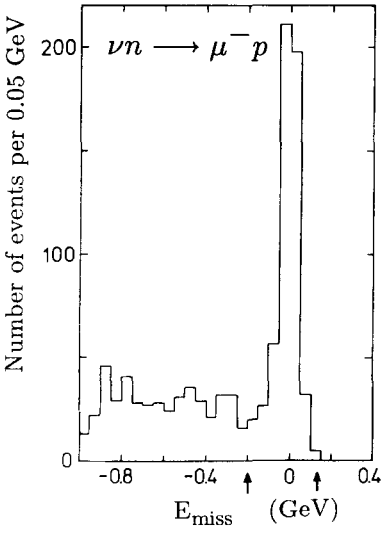

Fig. 1. Missing energy E_{miss} of candidates for reaction (1) with missing transverse momentum below 0.3 GeV/c. The arrows indicate the applied cuts.

TABLE 1
Corrected numbers of events and percentages of applied corrections.
All corrections are negative (see text).

Reaction	#	Events $W<2$ GeV/c^2	Events $W>2$ GeV/c^2	Corrections		
				accidental (%)	spectator (%)	background (%)
$\nu n \to \mu^- p$	(1)	552		1.2	–	
$\nu p \to \mu^- p\pi^+$	(2)	615		3.7	1.5	
$\bar{\nu} n \to \mu^+ n\pi^-$	(3)	981			–	26
$\bar{\nu} p \to \mu^+ p\pi^-$	(4)	620		9.3	–	
$\nu n \to \mu^- p\pi^0$	(5a)	251			–	12
$\nu n \to \mu^- n\pi^+$	(5b)	277			–	14
$\nu p \to \mu^- p\pi^+$	(6)		92	5.5	1.0	
$\bar{\nu} p \to \mu^+ p\pi^-$	(7)		158	2	–	
$\nu n \to \mu^- p\pi^+\pi^-$	(8)		260	2	–	
$\nu p \to \mu^- p\pi^+\pi^+\pi^-$	(9)		148	12	1	
$\bar{\nu} p \to \mu^+ p\pi^+\pi^-\pi^-$	(10)		163	6	<1	

protons can be recognized with nearly 100% efficiency. The efficiency decreases for momenta above 0.75 GeV/c. Kaons can only be recognized incidentally. For particles with momentum below 0.75 GeV/c that were not recognized as protons, no fit for that mass assignment was accepted. Table 1 shows the numbers of events passing the final kinematical criteria.

Events with the proper topological multiplicity but with additional neutral secondaries may accidentally pass the fit criteria. This background is mostly due to events with a single neutral pion in addition. The background has been investigated in all 3-constraint channels by studying the class of events with the next larger topological multiplicity. One pion was discarded and the kinematical procedure was applied to the remaining event. The percentages of this background are listed in the column "accidental" in table 1. The background is different for the various 3-constraint channels; it depends on the relative numbers of events in the observed and obscuring topology classes.

No background to 3-constraint events is expected from events with more than one neutral particle, so that no correction has been applied for these events.

4. Spectators

Special attention must be paid to events with a visible spectator proton. For the reactions $\nu n \to \mu^- p$ and $\nu n \to \mu^- p\pi^+\pi^-$ (1 and 8) events fitting an hypothesis with two outgoing protons are a genuine part of the sample:

$$\nu + d \to \mu^- + p + p_s\,, \tag{11}$$

$$\nu + d \to \mu^- + p + p_s + \pi^+ + \pi^-\,. \tag{12}$$

Most of these events are spectator events: the proton does not participate in the reaction but becomes visible as p_s by its Fermi motion. It generally has a momentum below 300 MeV/c and may be backward with respect to the beam direction. Fits are also obtained for events where the second proton is not a spectator, but results from rescattering in the deuteron. These events are also genuine examples of the reactions (1) and (8), although the kinematical quantities may be distorted.

For reaction $\nu p \to \mu^- p \pi^+$ (2), reaction (11) contributes to the background in the case the first proton is not recognized on the scanning table. This background is estimated by observing protons going backward with respect to the beam direction. Since in a single interaction scattering products can only go backward if their mass is below that of the target, backward protons in the odd-prong event samples are considered as genuine spectators (secondary protons of the $\nu/\bar{\nu}$ reactions being directed backwards due to Fermi motion in the deuteron are an exception to this rule).

From the set of backward spectators a set of forward spectator events is constructed by inverting the spectator direction and boosting the events to the new Lorentz frame. The constructed events obtain a weight factor

$$w = \left(\frac{1 - p_l/E}{1 + p_l/E} \right)^n , \tag{13}$$

where p_l is the (negative) momentum component of the spectator in the beam direction and E is the spectator energy. With $n = 2$ the weight factor accounts for the difference in beam flux as seen by particles moving in opposite directions and for the linear dependence of the total cross section on the beam energy. For the quasi-elastic channels under discussion, the cross section is constant with energy and the exponent $n = 1$ is used. Table 1 shows the percentages of events to be subtracted for this correction.

5. Neutrals in the final state

The reactions $\bar{\nu} n \to \mu^+ n \pi^-$ (3), $\nu n \to \mu^- p \pi^0$ (5a) and $\nu n \to \mu^- n \pi^+$ (5b) have a neutral particle in the final state and cannot be analyzed with kinematical fitting. The reactions are primarily recognized by their topology.

5.1. $\bar{\nu} + n \to \mu^+ + n + \pi^-$

The event candidates of reaction (3) are $\bar{\nu}$ 2-prong events with or without a spectator proton, where the negative particle is not identified as a kaon or a hyperon and where no neutral particles can be fitted to the primary vertex. Forward spectators may be constructed from the backward ones, as discussed in

sect. 4. The sample then contains events with a backward spectator and events created from them. An alternative method is to accept all forward protons with momentum below 300 MeV/c and all backward protons as spectators. Events that fit reaction (4) are not taken into account for the present channel. The two methods do not yield significantly different results.

Estimates of the background were made in two stages, using $\bar{\nu}$ 4-prong events:
(1) $\bar{\nu}$ 4-prongs were truncated by rejecting the positive and one negative hadron. A hypothetical neutron was added to the event and the analysis was performed as described before. Background distributions were obtained for all relevant quantities.
(2) The normalization of the background was obtained by means of the Lund Monte Carlo program by which deep inelastic events were generated [16, 18]. The ratio was determined between the number of 2-prong events satisfying the above criteria and the number of 4-prong events. This leads to a correction of 26% of the number of events with an effective neutron–pion mass below 2 GeV/c^2.

5.2. $\nu + n \to \mu^- + p + \pi^0$ AND $\nu + n \to \mu^- + n + \pi^+$

For reactions (5a) and (5b) an equivalent event selection and the same spectator procedure have been carried out as described in the previous section. Events were rejected when a fit without a neutral secondary could be obtained. In addition, events were rejected if they had a missing transverse momentum larger than 0.7 GeV/c. This cut does not affect genuine one-neutral-particle events, but largely reduces the background.

The problems of event separation and background subtraction are considerably more difficult for the two channels of this reaction than for any other interaction under investigation. First, a selection must be made of proton and pion tracks beyond the momentum limit where the estimate of the bubble density is effective. Failure of this selection leads to a proton–pion ambiguity. Secondly, a background subtraction must be applied to both channels making use of measured events that are again subject to this ambiguity.

In order to improve the proton–pion selection, use is made of the results of the mass-dependent fit in the geometry program. The program generally supplies track reconstruction fits for proton and pion masses for each positive track; the best fit may be used to choose the mass. The method has been tested with particle samples that had been identified by means of a kinematical fit.

For a number of events the pion hypothesis could be excluded because the event showed one or two secondary photons. With this argument, however, more-particle background events with a positive pion cannot be excluded. For some events, the π^+ channel could be rejected because it would lead to a backward going neutron. To the remaining ambiguous events (25% of the total) a neutron or π^0 was added and they were equally divided over the two channels.

The background subtraction has been performed as before by means of truncated 4-prong events. Two background samples were obtained by means of the beforementioned proton–pion separation method and by equally dividing the ambiguous events. The normalization of the background was again obtained from Monte Carlo calculations, taking into account the transverse momentum cut.

The percentages of background subtraction for reactions (3) and (5) are listed in table 1 in the column "background".

6. Physical variables

All physical quantities to be presented have been corrected bin-wise for background as discussed in the previous sections. EMI acceptance corrections, scanning corrections and (small) radiative corrections have been applied event by event. The following quantities are evaluated from the data:

(a) The effective mass W of a nucleon–pion system is obtained from the momenta of the two particles. In reactions (3) and (5) the neutral particle itself is not measured. Its parameters are derived from the muon, from the measured hadron and from the nominal neutrino direction. This leads to a slightly inferior experimental resolution as will be seen later in fig. 7b. The mass distribution of the Δ^- is wider than that of the Δ^{++}. A similar width as in fig. 7b can be obtained for reaction (2) when the outgoing proton is ignored and the effective mass is calculated from the remaining measured quantities.

(b) The squared 4-momentum transfer to the hadronic system Q^2 is obtained for all reactions in restricted areas of the effective mass. For reactions (6)–(10) the 4-momentum transfer squared t to the proton is calculated.

(c) For the decay-angle analysis of nucleon–pion systems, an expansion in spherical harmonics is performed in the proton–pion centre of mass system. The

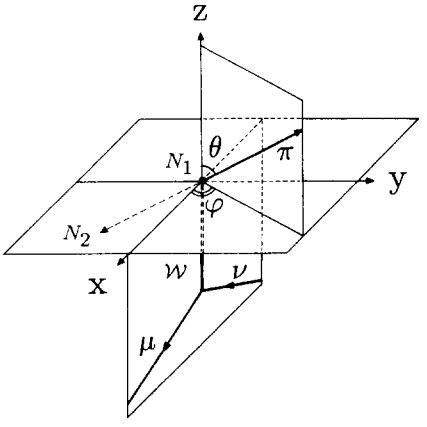

Fig. 2. Definition of the decay angles in the p–π c.m. system.

expansion is made in terms of the angle θ between the pion momentum and the z-axis and of the azimuthal angle φ of the pion momentum. The coordinate system is defined according to Adler [19] (see fig. 2): 1. The z-axis is in the direction of the momentum transfer to the hadronic system (direction of the heavy boson $\mathscr{W}$); 2. The x-axis is the projection of the muon momentum on a plane perpendicular to the z-axis; 3. The coordinate system is right handed.

Systematical errors are separately mentioned, all other quoted errors are statistical.

7. Cross sections

The determination of the cross sections for reactions (1)–(7) was performed by comparing event samples from these reactions with the complete charged current interaction samples of the experiment. These were then normalized to the world averages of the $\nu/\bar{\nu}$ nucleon cross sections [20]. The total cross section for an interaction of a $\nu/\bar{\nu}$ with a nucleon is proportional to the energy of the $\nu/\bar{\nu}$ whereas for the reactions just specified the cross section is independent of the $\nu/\bar{\nu}$ energy. At least this statement has to be verified in the energy region covered by this experiment.

$$N_{\text{total}} = \text{flux} \times \sigma_{\text{total}} \times E \times N_{\text{fid.vol.}}, \tag{14}$$

$$N_{\text{exclusive}} = \text{flux} \times \sigma_{\text{exclusive}} \times 0.5 \times N_{\text{fid.vol.}}, \tag{15}$$

The left-hand side of eqs. (14) and (15) are respectively the corrected total number of events and the corrected number of events for the reactions (1)–(7). The values for σ_{total} are 0.67×10^{-38} cm^2 for ν–N and 0.34×10^{-38} cm^2 for $\bar{\nu}$–N [20]. Both the $\nu/\bar{\nu}$ flux and the number of nucleons in the fiducial volume are the same in the two equations. The factor 0.5 in eq. (15) arises from the fact that the target particle for the exclusive reactions is either a proton or a neutron, whereas the total cross sections are values averaged over both nucleons in the deuteron.

The corrected number of events is obtained from the available measured number of events by applying several corrections. These corrections are not the same for the two categories N_{total} and $N_{\text{exclusive}}$ and are applied whenever possible on an event per event basis. Some corrections, however, can only be applied on a statistical basis. The following corrections were taken into account:

1. Smearing corrections have been applied to N_{total} for the loss of events at the lower cutoff value of the $\nu/\bar{\nu}$ energy spectrum and for the deformation of the y distribution. These effects are due to the uncertainty of the event energy determination. The statistically applied corrections follow closely the results obtained previously in this experiment [17].

2. In order to avoid errors in the muon identification, the analysis has been restricted to events with a muon momentum above 4 GeV/c. A correction is made

to N_{total} for this cut on a statistical basis. The correction for the exclusive channels is negligible.

3. Scanning losses were determined by comparing first and second area scanning results. Since the results of area scans are hardly independent, due to superposition of close tracks, badly illuminated regions in the chamber etc., a special independent track scan was performed on a restricted sample of the film. In this scan, the leaving muon, as taken from the BEBC EMI and IPF information, was followed back to verify if it came from an interaction. Indeed, the IPF scan showed that the traditional first-scan/second-scan procedure underestimated the losses by a factor 3. The correction for topology-dependent scanning losses was then applied to the complete sample on an event by event basis, incorporating the factor 3.

4. A passing rate correction is required for events which apparently do not obey charge conservation, could not be measured with sufficient accuracy or have a bad event data structure. The correction depends on the batch of film measured and was applied on an event by event basis.

5. The EMI geometrical acceptance correction depends essentially on the momentum and polar angle of the muon in the laboratory system. The correction factors are obtained by averaging over all vertex positions and azimuthal orientations of the muon. The correction is on an event by event basis.

6. The EMI electronic inefficiency correction accounts for the loss of CC events due to muons that fail to trigger the EMI. The correction is applied as a common factor for the whole sample.

7. The accidental EMI hits correction accounts for the probability that charged hadrons leaving BEBC are recorded as if they hit the EMI. This yields a correction of about -1.5%. This effect not only stems from hadron punch-through but also from spurious association. For the reactions (1)–(5) this correction was not applied since the two causes responsible for the effect are practically absent. The correction is applied as a common factor for the whole sample.

8. Corrections to the double differential cross section $\mathrm{d}^2\sigma/\mathrm{d}x\,\mathrm{d}y$ are calculated to account for the radiation of photons by the muon. The relative difference of observed and true cross sections gives a weight to each event dependent on the values of the scaling variables x and y.

9. The search for bare 1-prong events is not contained in the normal scanning procedure. These events occur in the $\bar{\nu}$–p interactions. In order to determine the contribution of these bare 1-prongs, part of the antineutrino film was scanned using a special procedure as described under point 3. This procedure yields 1-prong events (single μ^+) as well as many-prong events containing a μ^+. This correction amounts to $(11.8 \pm 0.8)\%$ of the total amount of charged current events.

Table 2 summarizes the average values of the listed corrections. The systematical errors on these corrections are estimated to be of the order of 20%. The errors quoted in table 3 contain the statistical errors of the samples of the exclusive channels, obtained after the corrections have been applied. For the cases the

TABLE 2
Average values of the cross section correction factors

Reaction		Factor	Reaction		Factor
$\nu N \to \mu^- X$	total	1.35	$\bar{\nu} N \to \mu^+ X$	total	1.44
$\nu n \to \mu^- p$	(1)	1.44	$\bar{\nu} n \to \mu^+ n\pi^-$	(3)	1.24
$\nu p \to \mu^- p\pi^+$	(2)	1.23	$\bar{\nu} p \to \mu^+ p\pi^-$	(4)	1.19
$\nu n \to \mu^- p\pi^0$	(5a)	1.25			
$\nu n \to \mu^- n\pi^+$	(5b)	1.29			

corrections have been obtained by means of Monte Carlo calculations, the Monte Carlo samples were large enough so as not to contribute to the errors.

For the total cross sections the partition of the corrections over the various categories has been published before [17]. For the exclusive channels it follows the same lines, although some corrections are absent (1-prongs, muon momentum cut, accidental EMI hits). The scanning loss correction is the most important one. It slightly varies with the reactions. Since corrections 1. and 2. depend on the energy spectrum of the $\nu/\bar{\nu}$ beams, the determination of the $\nu/\bar{\nu}$ cross sections was restricted to events produced in runs with the equivalent beam setting.

TABLE 3
Total cross sections of one-pion producing and quasi-elastic reactions. First line: this experiment; Second line: as deduced from reference [10]; Third line: Predictions of Rein and Sehgal [24, 25], see text.

		σ (10^{-38} cm^2)		
Reaction	Number	1.1 GeV/$c^2 < W <$ 1.4 GeV/c^2	1.4 GeV/$c^2 < W <$ 2.0 GeV/c^2	$W >$ 2.0 GeV/c^2
$\nu p \to \mu^- p\pi^+$	(2) (6)	0.54 ± 0.03	0.22 ± 0.02	0.12 ± 0.01
		0.55 ± 0.06	0.13 ± 0.03	0.094 ± 0.014
		0.493	0.205	–
$\bar{\nu} n \to \mu^+ n\pi^-$	(3)	0.53 ± 0.02	0.25 ± 0.02	–
		–	–	–
		0.441	0.238	–
$\bar{\nu} p \to \mu^+ p\pi^-$	(4) (7)	0.21 ± 0.01	0.32 ± 0.02	0.14 ± 0.01
		0.11 ± 0.03	0.19 ± 0.03	0.12 ± 0.02
		0.108	0.247	–
$\nu n \to \mu^- p\pi^0$	(5a)	0.19 ± 0.01	0.13 ± 0.01	–
		–	–	–
		0.116	0.162	–
$\nu n \to \mu^- n\pi^+$	(5b)	0.18 ± 0.01	0.20 ± 0.01	–
		–	–	–
		0.0676	0.234	–
$\nu n \to \mu^- p$	(1)		0.71 ± 0.03	

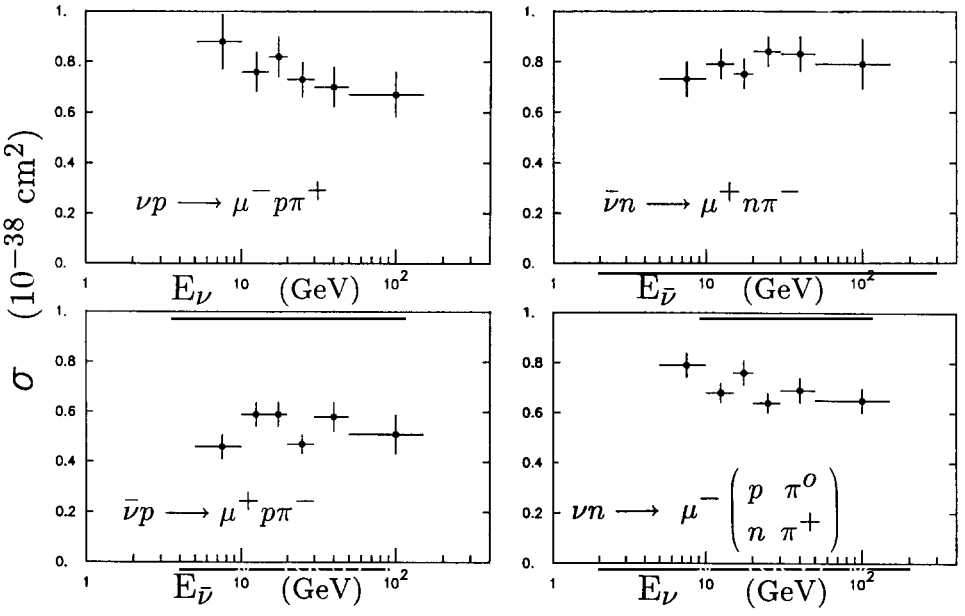

Fig. 3. Cross sections for reactions (2)–(5) as a function of the incident $\nu/\bar{\nu}$ energy; $W < 2$ GeV/c^2.

The cross sections are shown in table 3 and figs. 3–5. In the table they are compared with values obtained by Allen et al. [10] under similar conditions. Remarkable is the cross section for reaction (4) that is substantially larger in our determination than in theirs.

Although the 3-constraint fitting procedure is more complicated in deuterium than in hydrogen, we do not ascribe this result to an experimental effect in deuterium. Such an effect should be found in all fitted channels and be present at

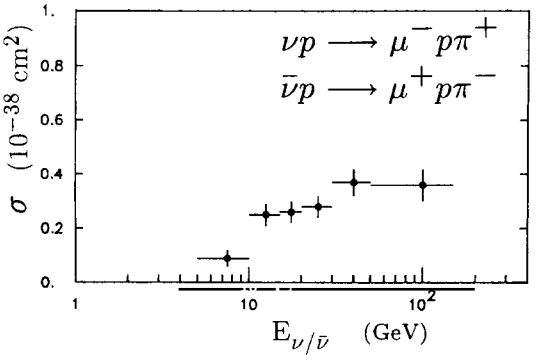

Fig. 4. Average cross section for reactions (6) and (7) as a function of $\nu/\bar{\nu}$ energy; $W > 2$ GeV/c^2.

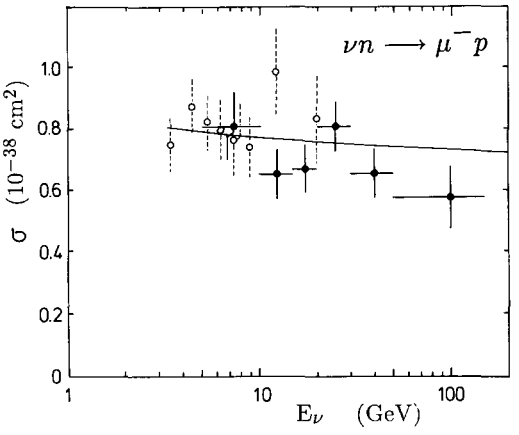

Fig. 5. Total cross section for quasi-elastic neutrino–neutron scattering as a function of neutrino energy. The results of Belikov et al. [5] are shown by open circles. The curve shows the parametrization according to eq. (17) with $M_A = 0.94$.

high- and low-W values. However, the observed discrepancy is limited to the low W-area in reaction (4) whereas at high W there is agreement between the two experiments. This agreement also exists in reactions (2) and (6) that are similar to (4) and (7). Moreover, an experimental effect would generally lead to a loss of events, not to an excess.

The results are also compared with the model predictions of Rein and Sehgal [25] which will be discussed in more detail in sect. 9. The agreement is sometimes good. For a few reactions the model underestimates our measured values, giving nearly a factor 3 difference for reaction (5b) at low values of W (< 1.4 GeV/c^2).

8. Quasi-elastic scattering

The total cross section for quasi-elastic scattering (reaction (1)) is found to be $(0.71 \pm 0.03) \times 10^{-38}$ cm^2 (table 3). The energy dependence of this cross section is shown in fig. 5. Fig. 6 shows the differential cross section distribution for the reaction. It has been corrected for scanning losses obtained with the special scanning procedure, as discussed in the previous section. Since the scanning losses are largest for events with a short proton track, the differential distribution becomes steeper after the correction.

The data have been analyzed according to the method proposed by Llewellyn-Smith [21]. A number of simplifying assumptions has been made: under the assumption of the validity of CVC and the absence of second class currents, all

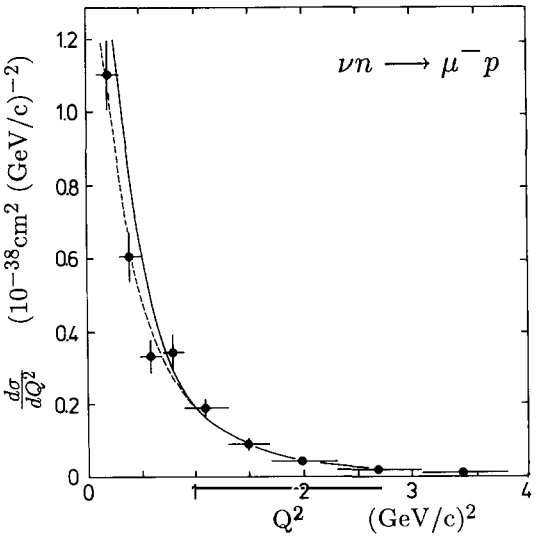

Fig. 6. Differential cross section of quasi-elastic neutrino scattering. Solid curve: Absolute prediction by means of eq. (17) with $M_A = 0.94$ GeV/c^2, Dashed curve: The shape of (17) with $M_A = 1.08$, normalized to the data.

form factors are real. The form factors F_v^3 and F_a^3 are set to 0. The form factors F_v^1 and ξF_v^2 are related to the electromagnetic form factors G_e^v and G_m^v by means of the isotriplet current hypothesis ($\xi = \mu_p - \mu_n$, the difference between the anomalous magnetic moments). The contributions of the order of m^2 are neglected (m is the muon mass). The electromagnetic form factors have a dipole shape with $M_v = 0.84$ GeV/c^2. The axial form factor F_a is parametrized according to:

$$F_a(Q^2) = F_a(0)\left(1 + Q^2/M_A^2\right)^{-2}, \tag{16}$$

with $F_a(0) = -1.2546$ as obtained from β-decay measurements [20]. Then, M_A is the only free variable. The differential cross section becomes

$$\frac{d\sigma}{dQ^2} = \frac{G^2 \cos^2 \vartheta_c M^2}{\pi E_\nu^2}\left[A(Q^2) - B(Q^2)\left(\frac{s-u}{M^2}\right) + C(Q^2)\left(\frac{s-u}{M^2}\right)^2\right], \tag{17}$$

where M is the nucleon mass. Actually, the form might be further simplified, since the values of $s - u = 4ME_\nu - Q^2 - m^2$ in the present experiment largely suppress the terms with A and the B, leaving only the third term between square brackets

with

$$C = \frac{1}{4}\left(|F_a|^2 + |F_v^1|^2 + \frac{Q^2}{M^2}\left|\frac{\xi F_v^2}{2}\right|^2\right) \tag{18}$$

as a prominent contribution.

The differential cross section (17) has been evaluated for the actual neutrino energy spectrum of the measured quasi-elastic events. It then has been fitted to the data as shown in fig. 6 in the Q^2 region above $Q^2 = 0.1$ (GeV/c)^2. The cut at low Q^2 has been made in order to reduce the influence of uncertainties in the scanning loss corrections and of nuclear effects in the deuteron.

The obtained best value is ($M_A = 0.94 \pm 0.07$) GeV/c^2, in agreement with the results of Belikov et al. [5] (1.00 ± 0.04) GeV/c^2, obtained at lower neutrino energy in a similar way. The result is shown by the solid curves in figs. 5 and 6. In addition, a separate test has been made on the shape of the Q^2 distribution. A maximum likelihood fit has been performed in the Q^2 interval between 0.1 (GeV/c)^2 and the maximum Q^2 of the events. This procedure yields a best value of ($M_A = 1.08 \pm 0.08$) GeV/c^2, resulting in the dashed curve in fig. 6. This value is in agreement with the values obtained with deuterium by Baker et al. [8] ((1.07 ± 0.06) GeV/c^2) and by Miller et al. [4] ((1.00 ± 0.05) GeV/c^2). These investigations only rely on the shape of the Q^2 probability distribution, not on a measurement of the cross section.

The discrepancy between the two values of M_A found in our experiment, indicates that according to eq. (17) the measured value of the cross section would lead to a steeper Q^2 distribution than actually observed.

Various authors [22, 23] have proposed alternative functions of Q^2 to replace the electromagnetic form factor. Such replacements given no improvement in our case, since they only make the form factor steeper. Assuming that the electromagnetic form factors are correct, we tend to the conclusion that parametrization by means of a single parameter, the axial dipole form factor, only leads to global agreement with the data, if both the cross section and the shape of the Q^2 distribution are taken into account.

9. One-pion production, baryon resonances

Fig. 7 shows the pion–nucleon effective mass W in the various neutrino and antineutrino channels. Figures a and b show that the channels (2) and (3) are largely dominated by the $\Delta^{++}(1232)$ and $\Delta^{-}(1232)$ resonances. The two diagrams are in striking agreement. The difference in experimental resolution has been explained in sect. 6. A weak indication exists for the production of $I = \frac{3}{2}$ resonances around 1.9 GeV/c^2.

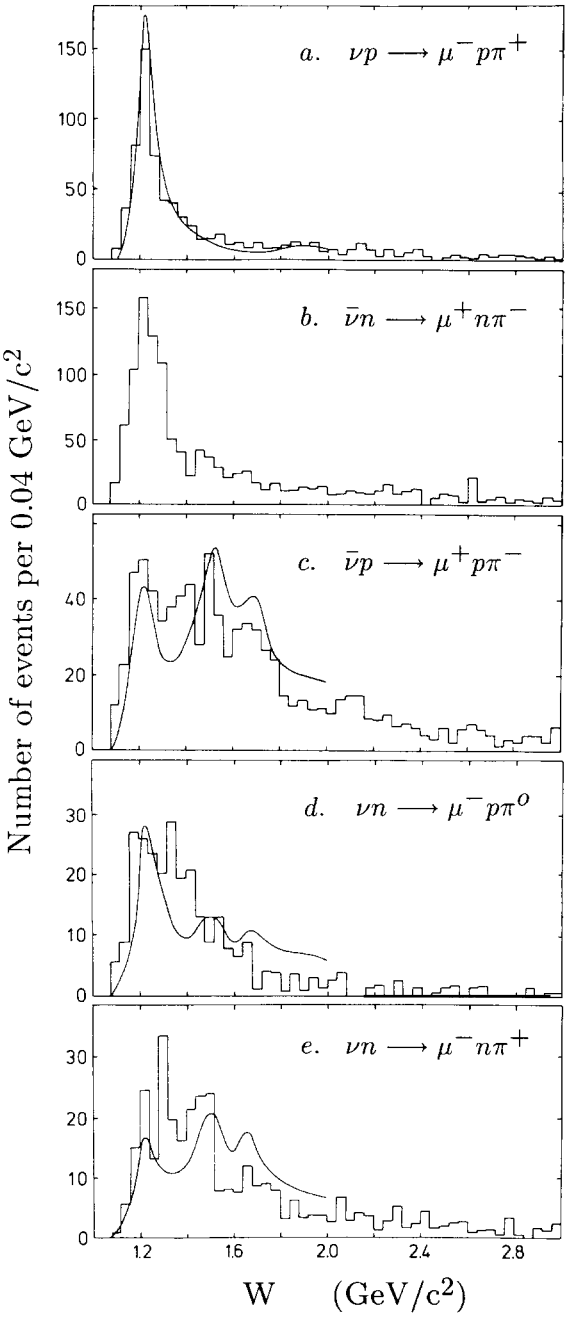

Fig. 7. Effective mass distributions for one-pion reactions. The curves are predictions of Rein [24], normalized to the number of events with 1.1 GeV/$c^2 < W <$ 2.0 GeV/c^2.

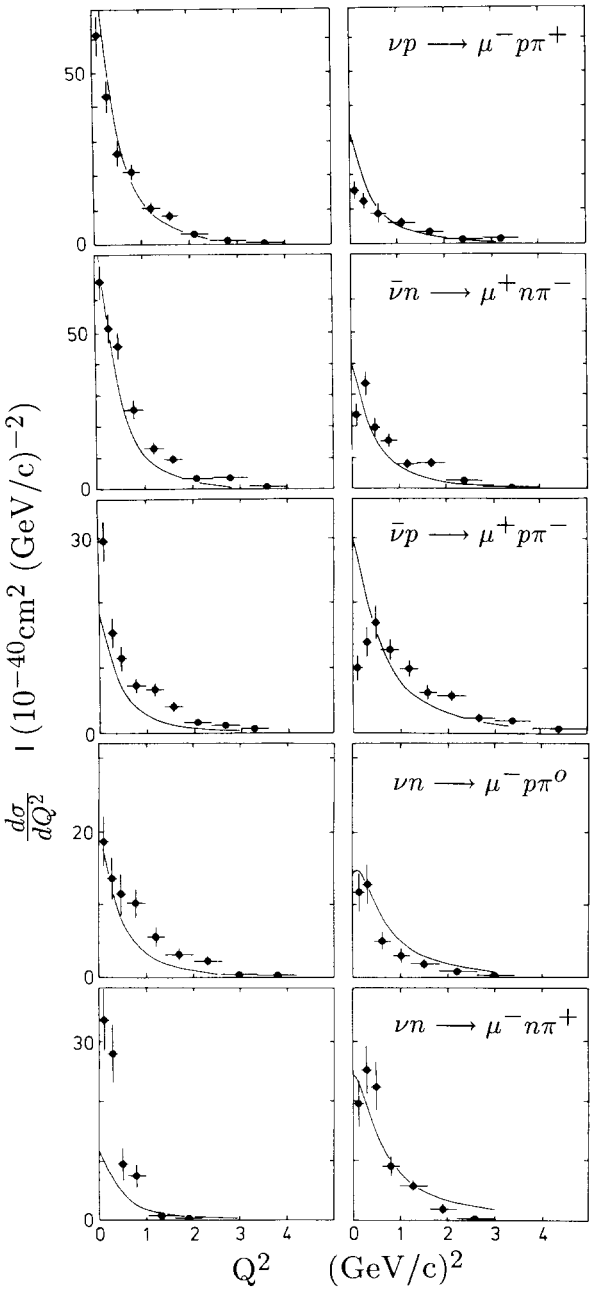

Fig. 8. Differential cross sections for one-pion reactions as a function of Q^2. Left: 1.1 GeV/c^2 < W < 1.4 GeV/c^2; Right: 1.4 GeV/c^2 < W < 2.0 GeV/c^2. The curves are the absolute predictions made with the model of Rein.

The mass and width of the $\Delta(1232)^{++}$ resonance have been determined in the mass interval between 1.10 and 1.35 GeV/c^2 by means of a likelihood analysis. The results for the 391 particles in this sample are $M_\Delta = 1.224 \pm 0.003$ GeV/c^2 and $\Gamma_\Delta = 0.090 \pm 0.007$ GeV/c^2. The mass, but more so the width, are lower than found in hadronic formation experiments ($\Gamma = 0.110 - 0.120$ GeV/c^2 [20]). This may be due to the existence of higher-order production diagrams in strong interactions that are absent in weak production processes.

In the other channels the existence of both $I = \frac{3}{2}$ and $I = \frac{1}{2}$ states becomes evident.

The differential cross sections as function of Q^2 are shown in fig. 8, for two intervals of the effective mass: $1.1 - 1.4$ and $1.4 - 2.0$ GeV/c^2. The distributions are similar for the various reactions and are definitely steeper for the lower than for the higher effective mass interval.

For ν–p and $\bar{\nu}$–p interactions, both Q^2 and W distributions are in good agreement with those obtained by Allen et al. [10] and Barish et al. [6] at comparable incident energies in hydrogen. The curves in the figures show the theoretical predictions made by Rein [24] on the basis of the quark model of Rein and Sehgal [25]. This model is an extension of the relativistic harmonic oscillator model of Feynman et al. [26]. It allows for the existence of various resonances in the different channels interfering with each other with pre-assigned phases. In addition there is a non-resonant non-interfering background.

All predictions are calculated for an incident $\nu/\bar{\nu}$ energy of 20 GeV with the value $M_A = 0.95$ GeV/c^2 of the axial form factor parameter. The curves in fig. 7 are normalized to the numbers of observed events in the W interval between 1.1 and 2.0 GeV/c^2; those of fig. 8 are absolute predictions. There is excellent agreement between the data and the prediction for the $I = \frac{3}{2}$ channels. In the other channels the agreement is less satisfactory. In general, the data are indicative of a relatively stronger production of low-mass resonances than predicted by the model, predominantly of the $\Delta(1232)$ resonance. This evidence is also shown by the cross section values of table 3. There is general agreement between the data and the absolute predictions for the cross sections in fig. 8, with the exception of the striking disagreement in the diagrams for reactions (4) and (5b) at low W. The shapes of the Q^2-distributions are in global agreement, but the measured cross sections exceed the predicted ones by a sizeable amount.

The decay angular distributions of the nucleon–pion system are investigated by means of a spherical harmonics expansion. For the $p\pi^+$ system in reaction (2) the results are shown in table 4. All sperical harmonics are in units of $Y_0^0 = 1/\sqrt{4\pi}$. The resulting spin density matrix elements for the $p\pi^+$ channel are shown in fig. 9, together with the predictions of Rein and Sehgal [24, 25]. The matrix element $\tilde{\rho}_{33}$ demonstrates the predominance of the $\Delta^{++}(1232)$-resonance in the low-effective mass region. The fall-off of the curve at higher mass is due to the presence of other $I = \frac{3}{2}$ resonances or, possibly, of a non-resonance amplitude. The values for

TABLE 4
Mean values of spherical harmonics for the $p-\pi^+$ system in different W-intervals. The angles θ and ϕ are defined in fig. 2.

W (GeV)	1.1–1.18	1.18–1.23	1.23–1.28	1.28–1.5	1.5–1.7	1.7–2.0
$\langle Y_1^0 \rangle$	-0.22 ± 0.11	-0.01 ± 0.07	0.29 ± 0.09	0.32 ± 0.09	0.61 ± 0.13	0.84 ± 0.13
$\langle Y_2^0 \rangle$	-0.06 ± 0.12	-0.13 ± 0.07	-0.19 ± 0.10	-0.08 ± 0.09	0.49 ± 0.15	0.80 ± 0.14
$\langle \Re Y_1^1 \rangle$	0.21 ± 0.09	-0.02 ± 0.06	-0.20 ± 0.08	-0.05 ± 0.06	0.12 ± 0.08	-0.03 ± 0.07
$\langle \Im Y_1^1 \rangle$	-0.09 ± 0.08	-0.06 ± 0.06	-0.06 ± 0.08	0.01 ± 0.06	-0.08 ± 0.09	-0.17 ± 0.09
$\langle \Re Y_2^1 \rangle$	0.26 ± 0.08	0.05 ± 0.06	0.02 ± 0.08	0.00 ± 0.06	0.09 ± 0.07	-0.05 ± 0.06
$\langle \Im Y_2^1 \rangle$	0.07 ± 0.07	0.00 ± 0.05	0.16 ± 0.08	-0.01 ± 0.06	-0.04 ± 0.08	-0.03 ± 0.07
$\langle \Re Y_2^2 \rangle$	-0.04 ± 0.07	0.08 ± 0.05	0.08 ± 0.07	0.04 ± 0.06	0.09 ± 0.09	-0.08 ± 0.09
$\langle \Im Y_2^2 \rangle$	-0.07 ± 0.08	-0.07 ± 0.05	-0.01 ± 0.08	0.06 ± 0.06	-0.15 ± 0.08	-0.03 ± 0.07

$\tilde{\rho}_{33}$ are rather well described by the model of Rein. Those for $\tilde{\rho}_{3-1}$ are systematically off the model predictions.

Table 5 shows the results of the expansion for the $p\pi^-$ system in reaction (4). There is only global and qualitative agreement with the previous results of Allen et al. for the same reaction. There is a marked disagreement for the coefficient Y_1^0 between the two experiments. The agreement with the predictions of Rein is good

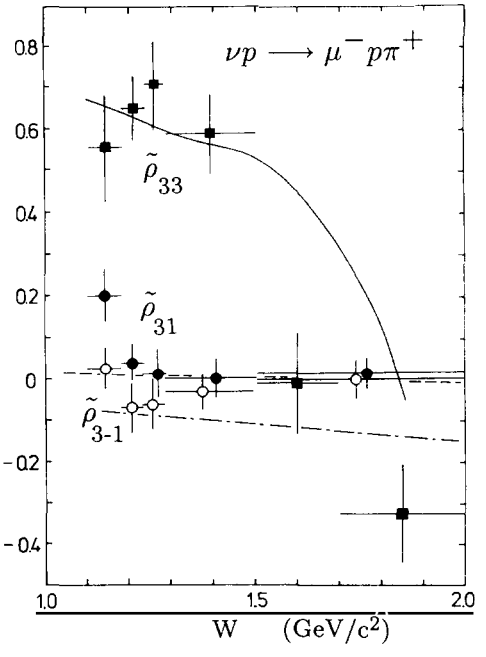

Fig. 9. Spin density matrix elements $\tilde{\rho}_{33}$ (squares), $\tilde{\rho}_{31}$ (full circles) and $\tilde{\rho}_{3-1}$ (open circles) for the $p\pi^+$ system as a function of W. Also shown are the predictions of Rein [24]: solid curve $\tilde{\rho}_{33}$, dashed curve $\tilde{\rho}_{31}$ and dashed–dotted curve $\tilde{\rho}_{3-1}$.

TABLE 5
Mean values of spherical harmonics for the proton–π^- system in different W-intervals. The angles θ and ϕ are defined in fig. 2.

W (GeV)	1.0–1.2	1.2–1.4	1.4–1.6	1.6–1.8	1.8–2.0
$\langle Y_1^0 \rangle$	0.20 ± 0.13	0.26 ± 0.11	0.36 ± 0.12	0.35 ± 0.07	0.68 ± 0.06
$\langle Y_2^0 \rangle$	0.10 ± 0.14	-0.08 ± 0.12	-0.07 ± 0.12	0.10 ± 0.08	0.43 ± 0.07
$\langle \Re Y_1^1 \rangle$	0.02 ± 0.09	-0.04 ± 0.09	-0.05 ± 0.09	-0.01 ± 0.05	-0.04 ± 0.04
$\langle \Im Y_1^1 \rangle$	-0.05 ± 0.09	0.09 ± 0.03	-0.26 ± 0.09	-0.13 ± 0.05	-0.15 ± 0.04
$\langle \Re Y_2^1 \rangle$	-0.07 ± 0.09	0.04 ± 0.09	-0.07 ± 0.10	-0.02 ± 0.05	-0.01 ± 0.04
$\langle \Im Y_2^1 \rangle$	-0.02 ± 0.09	-0.18 ± 0.09	-0.01 ± 0.10	0.01 ± 0.05	0.12 ± 0.04
$\langle \Re Y_2^2 \rangle$	-0.02 ± 0.10	0.03 ± 0.09	-0.05 ± 0.10	-0.04 ± 0.05	0.15 ± 0.04
$\langle \Im Y_2^2 \rangle$	-0.04 ± 0.09	0.20 ± 0.09	-0.07 ± 0.09	-0.01 ± 0.05	-0.02 ± 0.04

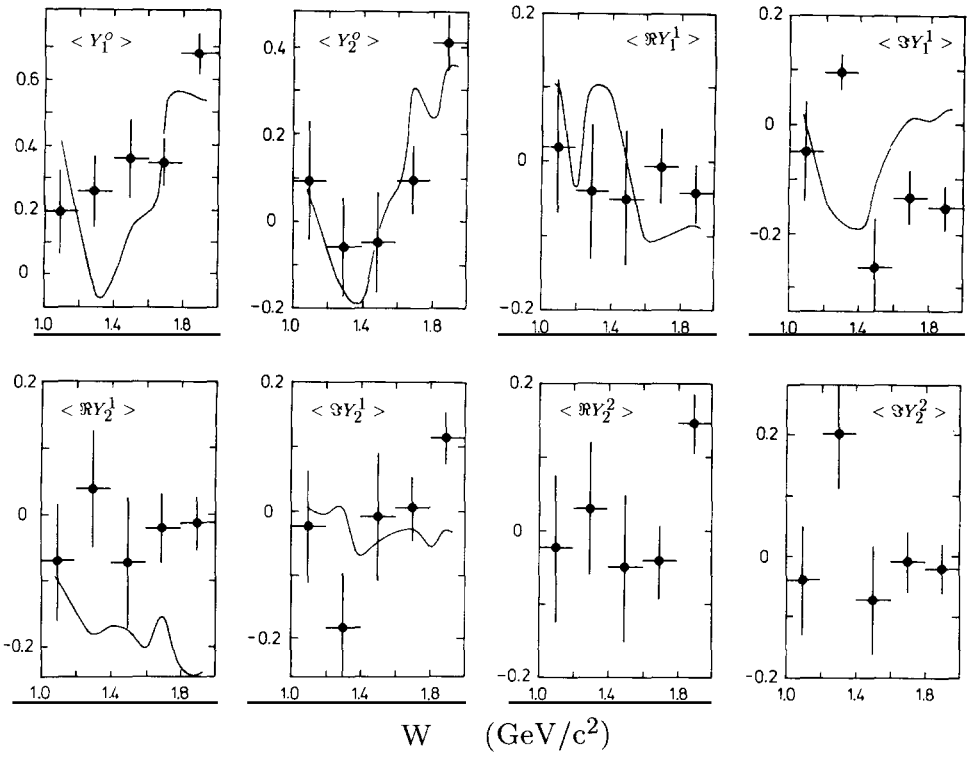

Fig. 10. Average values of the spherical harmonics for the $p\pi^-$ system in reaction (4). The curves show the predictions of Rein [24].

for Y_2^0, as it was for the previous reaction. The agreement is poor in the case of the other coefficients, as shown in fig. 10.

10. Pion production at low momentum transfer

The meson production reactions (6)–(10) are all 3-constraint channels with a proton in the final state. For the one-pion production reactions (6) and (7) an additional condition $W > 2$ GeV/c^2 has been imposed, in order to exclude the previously discussed resonance production. The events of the reaction samples with more pions automatically fulfill this condition. However, resonances of the baryon with one of the pions are still present in the selected samples. Fig. 11 shows the distributions of t, the squared momentum transfer to the nucleon. For the three reactions, the distributions fall off rapidly with increasing t, t being largely restricted to values below 1 (GeV/c)^2. As a consequence, the protons of the events can be recognized on the scanning table and no proton–pion ambiguity occurs in the kinematics procedure.

In spite of the preference for low t-values as demonstrated in fig. (11), the distributions are not steep enough to be explained by a diffractive production mechanism of the pion or the 3-pion system. Instead of a slope parameter $b \approx$

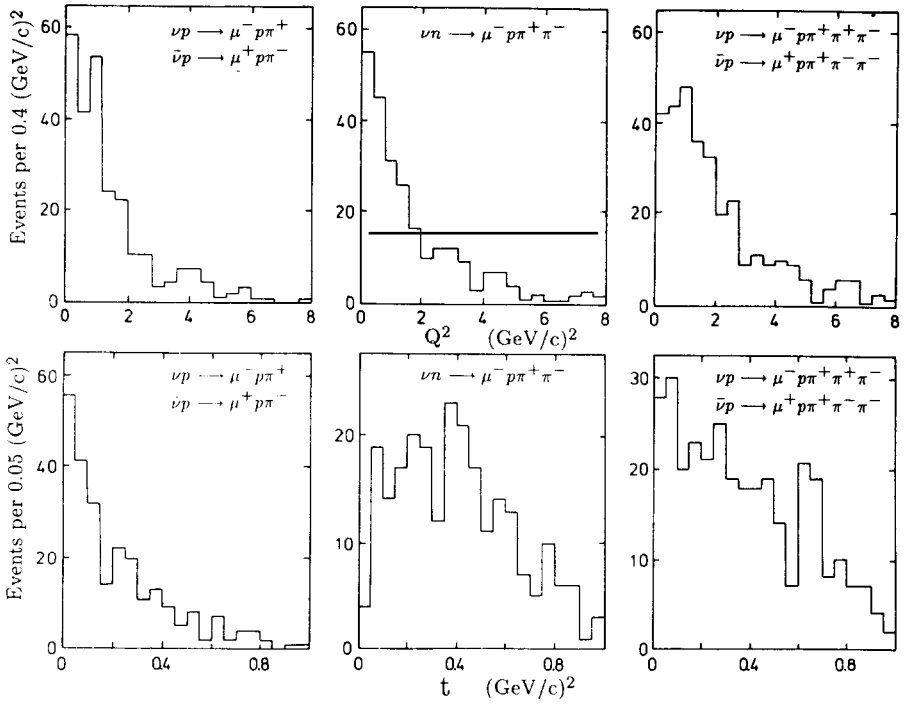

Fig. 11. Q^2 and t-distributions of single- and multi-pion production.

9 $(\mathrm{GeV}/c)^2$ in $\mathrm{d}\sigma/\mathrm{d}Q^2 \propto \exp(-bt)$, as expected for diffractive single-nucleon reactions, b-values of 4.5 and 2.7 $(\mathrm{GeV}/c)^2$ are obtained for the 1-pion and 3-pion channels respectively. The t behaviour of the charge exchange interaction (8) is remarkable: it seems to be indicative of a more complicated production mechanism, giving rise to a less peripheral collision than in the other channels.

Fig. 11 also shows the Q^2 distributions for the three reactions. The t and Q^2 histograms for the individual ν and $\bar{\nu}$ channels of the one-pion and three-pion production are very similar. In order to obtain higher statistics, $\nu/\bar{\nu}$ data have been combined for this analysis.

10.1. ONE-PION PRODUCTION

The one-pion production has been investigated for the ν- and $\bar{\nu}$-induced channels (reactions (6) and (7)). The topology of reaction (6) is identical with that of (2), but here events are selected with an effective proton–pion mass larger than 2 GeV/c^2. In the same way reactions (4) and (7) are equivalent. The fitting procedure, event selection and background subtraction are as discussed before.

The events in the two channels are $(0.35 \pm 0.04)\%$ and $(0.95 \pm 0.07)\%$ of the total $\nu/\bar{\nu}$ charged current events. The individual cross sections are presented in table 3. As a function of $\nu/\bar{\nu}$ energy the combined cross section is rising throughout the whole investigated energy range (fig. 4), with a possible saturation at high energies. The cross section values, the t and Q^2 distributions are compatible with the results of Allen et al. [10]. These authors have already pointed out that the t distribution may be explained by the one-pion Regge exchange.

10.2. TWO-PION PRODUCTION

Fig. 12 shows the effective mass distribution of the 2-pion system for the charge exchange reaction (8). The figure shows copious production of the ρ^0. There is some evidence for the presence of the $f(1270)$. The shape of the background behind the ρ^0 meson was estimated from the smoothed two-pion effective mass distribution of the reaction $\bar{\nu}\mathrm{n} \to \mu^+\mathrm{p}\pi^-\pi^-$. This procedure is justified by the inspection of the $\mathrm{p}\pi^+\pi^-$ Dalitz plot that shows little overlap between ρ^0–p and Δ^{++}–π^- candidates. The estimated background and the superimposed resonance are shown in the figure. After correction for the invisible decays of the ρ^0, the number of ρ^0 events is 75 ± 18, corresponding to a cross section of $(0.08 \pm 0.02) \times 10^{-38}$ cm^2. The presence of an important non-resonant background in fig. 12 indicates that more than one production mechanism is active in the channel. The t distribution with its dip towards $t = 0$ supports this conclusion.

10.3. THREE-PION PRODUCTION

In reactions (9) and (10) the production of the axial vector meson A1(1260) is expected to occur. In order to increase the A1 signal compared to the non-reso-

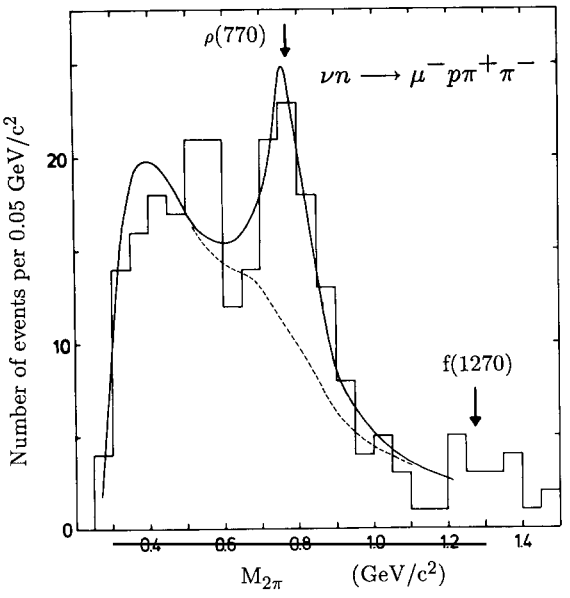

Fig. 12. Two-pion effective mass distribution for reaction (8). The full curve shows the ρ^0 resonance superimposed on the estimated background. The dotted curve shows the background alone.

nant 3-pion background, use is made of the fact that the A1 nearly exclusively decays into $\rho\pi$ [20]. A selection of events has been made where the effective mass of one of the $\pi^+\pi^-$ combinations satisfies the condition $0.47 < M^2_{\pi\pi} < 0.78$ $(\mathrm{GeV}/c^2)^2$. The effective mass distribution of the 3-pion system for the reduced sample is shown in fig. 13. Inspection of the Dalitz plot of the $p\pi\pi$ system shows the presence of a $\Delta(1232)$–π signal in the channel that partly overlaps the A1 mass region. If events in a band of ± 50 MeV/c^2 around the Δ mass are removed, the 3-pion effective mass histogram reduces to the shaded area in the figure. Indeed, an A1 signal becomes visible after these cuts have been made.

The weighted numbers of events corrected for the applied cuts and for kinematical effects are 94 for ν and 90 for $\bar{\nu}$ $(0.34 \pm 0.03)\%$ resp. $(0.53 \pm 0.06)\%$ of the total charged current $\nu/\bar{\nu}$ events. This results in a combined cross section of $(0.18 \pm 0.04) \times 10^{-38}$ cm^2, averaged over the $\nu/\bar{\nu}$ incident energy interval.

A theoretical estimate of the A1 production cross section in neutrino reactions is made by Gaillard et al. [27] on the basis of a diffractive vector meson dominance model. If the initial assumption about the axial coupling constant of the A1 to the vector boson is replaced by a value estimated from $\tau \to \nu 3\pi$ decay [28], the model predicts a number of events considerably larger than the observed value. However, a comparison seems not relevant since our experimental results do not comply with

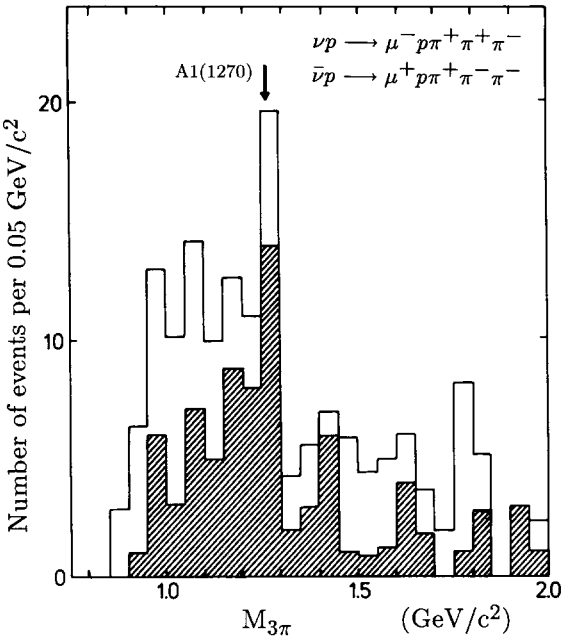

Fig. 13. 3-pion effective mass distribution for reactions (9) and (10). One $M_{\pi^+\pi^-}$-value lies in the ρ^0 band; for shaded events $M_{p\pi^+}$ lies outside the Δ^{++} band.

some of the basic features of the model. In particular, if the observed event signal is to be attributed to the A1(1260), this resonance is not diffractively produced. For the t distribution of the shaded events in fig. 13 below the effective mass of 1.6 GeV/c^2 a slope parameter $b = 3.4$ (GeV/c)$^{-2}$ is obtained. Moreover, the experiment shows saturation of the cross section at higher $\nu/\bar{\nu}$ energy, which is not yet incorporated in the model.

Conclusion

Measurements have been performed on the cross section and Q^2 dependence of quasi-elastic neutrino–neutron charged current scattering. A discrepancy is found between the experimental results and the common theoretical description.

The production of nucleon–pion systems has been investigated in the various $\nu/\bar{\nu}$–p/n channels. Effective mass histograms, Q^2 dependencies and decay angular distributions have been obtained. At effective mass below 2.0 GeV/c^2 the reactions are dominated by the production of baryon resonances, in global agreement with theoretical descriptions, in particular those of Rein and of Rein and Sehgal. Some specific discrepancies between the measurements and these predictions have been found. Values are presented for the mass and width of the $\Delta^{++}(1232)$ resonance, different from the ones found in hadronic experiments.

The production of one- and more-pion systems without baryon excitation proceeds at low momentum transfer to the target. Resonance signals of ρ^0 and A1(1260) are observed in the final states. The momentum transfer spectra of the reactions exclude simple diffractive mechanisms and simple one-pion exchange in the two-pion production channel.

Cross sections at several energies have been measured for all reactions under study. Most cross sections are found to be independent from the incident energy between 5 and 200 GeV.

The authors are indebted to the CERN staff for running the SPS and BEBC and to the scanning personnel in their home institutes. They thank Dr. D. Rein, Aachen, for many illuminating discussions and for supplying the predictions of his model adapted to the special conditions of this experiment.

References

[1] S. Bonetti et al., Nuovo Cimento A38 (1977) 260
[2] S.J. Barish et al., Phys. Rev. D16 (1977) 3103
[3] N.J. Baker et al., Phys. Rev. D23 (1981) 2499
[4] K.L. Miller, Phys. Rev. D26 (1982) 537
[5] S.V. Belikov et al., Z. Phys. A320 (1985) 625
[6] S.J. Barish et al., Phys. Lett. B91 (1980) 161
[7] V.V. Makeev et al., Pis'ma Zh. Eksp. Teor. Fiz. 34 (1981) 418
[8] N.J. Baker et al., Phys. Rev. D23 (1981) 2495
[9] G.M. Radecky et al., Phys. Rev. D25 (1982) 1161
[10] P. Allen et al., Nucl. Phys. B264 (1986) 221
[11] T. Kitagaki et al., Phys. Rev. D34 (1986) 2554
[12] G.T. Jones et al., Z. Phys. C43 (1989) 527
[13] H.J. Grabosch et al., Z. Phys. C41 (1989) 527
[14] D. Day et al., Phys. Rev. D28 (1983) 2714
[15] D. Allasia et al., Z. Phys. C20 (1983) 95
[16] Sylvia Barlag, Quasielastic interactions and one-pion production by neutrinos and anti-neutrinos on a deuterium target, Thesis, Amsterdam (1984)
[17] D. Allasia et al., Nucl. Phys. B239 (1984) 301
[18] G. Ingelman, T. Sjöstrand, A Monte Carlo program for lepto-production, Univ. of Lund, LU TP 80-12;
T. Sjöstrand, Comput. Phys. Commun. 27 (1982) 243
[19] S.L. Adler, Ann. Phys. (N.Y.) 50 (1968) 89
[20] Particle Data Group, Phys. Lett. B204 (1988) 1
[21] C.H. Llewellyn-Smith, Phys. Rep. 3 (1972) 261
[22] L.M. Sehgal, Proc. of the EPS Int. Conf. High energy physics, Geneva (1979) 98
[23] M.G. Olsson et al., Phys. Rev. D17 (1978) 2938
[24] D. Rein, Ein-Pion Erzeugung in Neutrino-Reaktionen, RWTH Aachen 86/13, 1986;
D. Rein, Z. Phys. C35 (1987) 43
[25] D. Rein and L.M. Sehgal, Ann. Phys. (N.Y.) 133 (1981) 79
[26] R.P. Feynman, M. Kislinger and F. Ravndal, Phys. Rev. D3 (1971) 2706
[27] M.K. Gaillard, S.A. Jackson and D.V. Nanopoulos, Nucl. Phys. B102 (1976) 326;
M.K. Gaillard and C.A. Piketty, Phys. Lett. B68 (1977) 267
[28] P.R. Burchat, Proc. XXIIIth Int. Conf. on High energy physics, Berkeley (1986) 756